

Beam Steering Reconfigurable Compact Antenna Based on Hybridization between Split Ring Resonators

Kammel Rachedi¹, Julien de Rosny¹, Yvan Kokar²,
Dinh Thuy Phan-Huy³, and Abdelwaheb Ourir^{1, *}

Abstract—Reconfigurable antennas that are able to provide a high spatial diversity are increasingly adopted in many wireless applications. An original design of a planar printed compact antenna that achieves an electronically controlled beam steering by using metamaterial hybridization is presented in this paper. The designed antenna, made of coupled split ring resonators, is able to switch between 8 radiation patterns steering in 8 different directions at the working frequency of 2.45 GHz. The spatial diversity is assessed from the analysis of the correlation matrix between the patterns. This concept would provide a promising and compact solution for green telecommunication systems.

1. INTRODUCTION

Reconfigurable antennas present a good trade-off between multipoint antenna that implies a complex radio-frequency control and single port antenna that suffers from a lack of spatial agility. The design of such antennas can be based on a U-slot [1], cubic [2] and patch structures [3,4]. Reconfigurable metamaterials also provide an interesting solution. In [5], the use of metamaterials, composed of planar metallic patterns periodically organized driven by varactors allows frequency tuning associated with a strong pattern diversity. Metamaterial antenna based on split ring resonators (SRR) has also attracted a lot of interest [6] because SRR has the property to elicit a high resonant frequency with a subwavelength size [7]. As a consequence, SRRs have been used for designing small compact antennas due to the inductive loading of the main radiating element [8]. Because the resonant frequency of the SRR can be relatively easily tuned by lumped elements, SRRs can be employed to adjust the working frequency of antennas [9] or controlling the resonance inside the magnetic metamaterial [10]. In [11], it has been observed that a planar antenna made of strongly coupled SRRs and tuned by varactors can generate a large number of radiation patterns. In the present work, this property is leveraged to design a small etched reconfigurable antenna based on a double SRR fed by an RF source. This last is affected by 4 reconfigurable parasitic SRR in its vicinity. The hybridization process in such structures leads to modes splitting. Some of them are able to generate a directional radiation pattern associated with a good impedance matching. To reconfigure the antenna, PIN diodes have been placed within the parasitic SRR to tune their resonance frequencies. The next section of the paper is devoted to the introduction of a simple model to explain the hybridization effect between 2 SRRs. Then the full design of the antenna is described. The design is tested numerically with a full-wave simulation software. A prototype is built and characterized. Finally, we quantify the spatial diversity of this antenna and discuss its application for an original communication scheme only based on this property.

Received 10 February 2020, Accepted 25 March 2020, Scheduled 27 April 2020

* Corresponding author: Abdelwaheb Ourir (a.ourir@espci.fr).

¹ Institut Langevin, ESPCI Paris, CNRS, PSL University, 1 rue Jussieu, Paris 75005, France. ² UBL, INSA, IETR, UMR-6164, France. ³ Orange Gardens, 44 Avenue de la République, Châtillon 92320, France.

2. MODE HYBRIDIZATION PRINCIPLE

In order to illustrate the effect of this hybridization process on the radiated field, we use a simple magnetoelectric dipolar model that was presented in detail in [11]. This model is here applied to a double SRR excited by RF voltage source. A simple SRR is in the near field of the double SRR. The double SRR is assumed to be well approximated by a magnetic dipole \mathbf{m}_s . The orientation of this vector is normal to the ring plane as illustrated on Fig. 1(a). As a consequence, this antenna provides an omnidirectional radiation pattern in the E -plane and shows a high reflection coefficient at the resonant frequency of 2.4 GHz. A parasitic SRR is then placed in the direct vicinity of the main radiating element as illustrated in Fig. 1(c). This parasitic element behaves as a magneto-electric resonator characterized by its magnetic moment \mathbf{m}_p and its electric moment \mathbf{p}_p as illustrated.

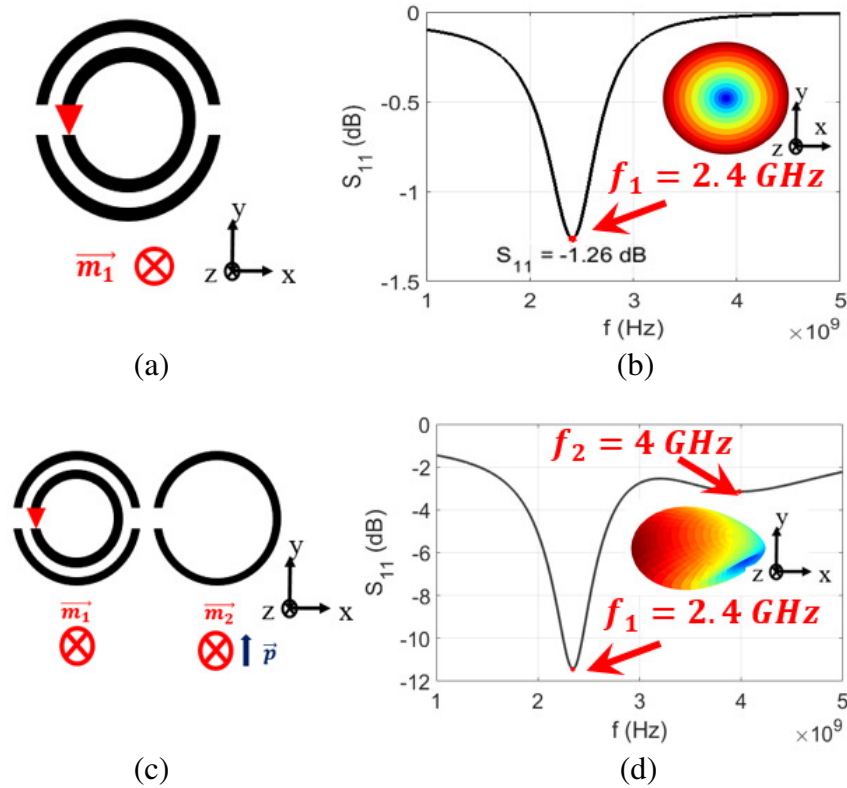


Figure 1. (a) Geometry of the double Split Ring Resonator (SRR). The red triangle represents the voltage source. (b) Calculated reflection coefficient and radiation pattern at the resonant frequency. (c) Schematic view of the coupled resonator systems. (d) Calculated reflection coefficient of the coupled system and its radiation pattern at 2.4 GHz.

The 3 moments can be expressed in terms of the complex amplitude of the currents I_s and I_p flowing in the double and in the parasitic SRRs, respectively:

$$\mathbf{m}_s = S_s I_s \mathbf{u}_z, \quad (1)$$

$$\mathbf{m}_p = S_p I_p \mathbf{u}_z, \quad (2)$$

$$\mathbf{p}_p = \frac{d_p I_p}{j\omega} \mathbf{u}_d. \quad (3)$$

where S_s and S_p are the equivalent surfaces of the magnetic dipoles of the double SRR source and the parasitic SRR, respectively, and d_p stands for the equivalent length of the electric dipole of the parasitic SRR.

Based on the dyadic Green's function formalism, the mutual impedance Z_{sp} between the 2 structures (double SRR & parasitic SRR) can be worked out analytically [11]. The impedance Z_{eq} seen at the input port of the double SRR is then deduced from the matrix equation:

$$\begin{pmatrix} Z_{ss} & Z_{sp} \\ Z_{sp} & Z_{pp} \end{pmatrix} \begin{pmatrix} 1 \\ I_p \end{pmatrix} = \begin{pmatrix} Z_{eq} \\ 0 \end{pmatrix}$$

where Z_{ss} and Z_{pp} are the self-impedances of the double and parasitic SRRs, respectively. It is assumed that they behave as an RLC circuit near their fundamental resonance. The RLC parameters are adjusted manually by comparing the reflection coefficient to the one carried out with a full-wave software (Time domain solver of the commercial software CST Studio).

Based on this model, the reflection coefficients and the radiation patterns at the main resonant frequency (2.4 GHz) have been calculated (see Figs. 1(b) and 1(d)). While the excited double SRR shows a single main magnetic resonance (Fig. 1(b)), the second structure composed of the two coupled resonators provides two resonances as illustrated in Fig. 1(d). In the first case, the double SRR structure has a high reflection coefficient (-1.3 dB) at the operating frequency. In the second case, a low reflection coefficient meaning a good radiation efficiency ($S_{11} < -10$ dB) is clearly observed at 2.4 GHz. This phenomenon is due to the hybridization effect widely studied during the last years in such metamaterial based structures [11]. Moreover, the mode now generates a directional radiation lobe as illustrated in the inset of Fig. 1(d). The added resonator seems to behave as a Yagi-Uda reflector. The main difference is that this subwavelength SRR is placed in the near-field region of the double SRR, while the reflector is placed at a quarter wavelength distance in a classical Yagi-Uda configuration. Here, a phase shift between the currents flowing on both cells causes the omnidirectional pattern to be more directive.

3. DESIGN AND OPTIMIZATION OF THE RECONFIGURABLE ANTENNA

In order to design a beam-steerable antenna, this hybridization phenomenon is leveraged. Fig. 2(a) shows the proposed design. To minimize the losses, the circuit is etched on a low loss substrate ($\epsilon_r = 2.6$ and $\tan \delta = 0.0019$ at 2.0 GHz). The double SRR that is used as a main radiator is now surrounded by 4 parasitic SRRs. A tapered balun that feeds the external ring of the double SRR is used to test our antenna prototype as illustrated in Fig. 2(a). To control these 4 sub-wavelength resonators, switching components should be inserted within the gap of each parasitic loop. In [12], different kinds of switching components are discussed. As the reconfiguration of the antenna implies a change of the surface current distribution, lumped elements like Radiofrequency Microelectromechanical Systems (RF MEMS) [13], PIN diodes [14], Varactors [15], or Optical Switches [16] can be used. The need for high data rate implies a fast switching process. For this reason, we choose to use PIN diodes. The radius and gap size of the parasitic element are adjusted to be close to the fundamental resonance of the double SRR when the PIN diode is forward biased. When the PIN diode is reverse-biased, the diode acts as an open circuit. The resonance frequency of the parasitic SRR is higher and only weakly interacts with the main mode of the double SRR. Biasing forward one or two consecutive diodes leads to 8 interesting radiation patterns (see Table 1).

Table 1. Biasing (F: Forward; R: Reverse) of the 4 diodes for the 8 states of the reconfigurable antenna.

	1	1-2	2	2-3	3	3-4	4	4-1
D_1	F	F	R	R	R	R	R	F
D_2	R	F	F	F	R	R	R	R
D_3	R	R	R	F	F	F	R	R
D_4	R	R	R	R	R	F	F	F

The diode switching changes not only the radiation pattern but also the antenna matching. The SRR geometry is optimized using a full-wave simulation software (Microwave CST, 2019) so that all the 8 reflection parameters (S_{11}) corresponding to the 8 diode states are sufficiently low at 2.45 GHz. The optimal dimensions are shown on Fig. 2(b). A good matching is obtained for the 8 states with a

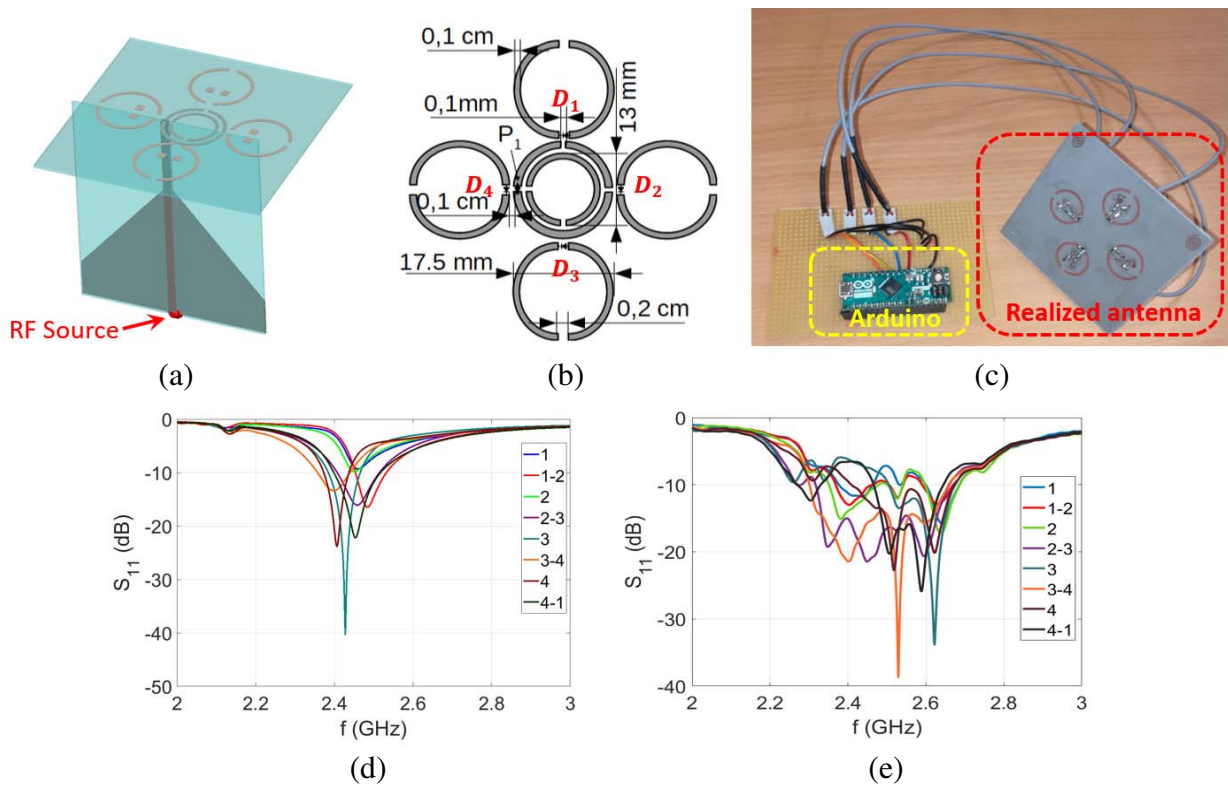


Figure 2. (a) Schematic view of the reconfigurable SRR antenna. A microstrip taper balun is used to feed the outer ring of the double SRR. (b) Dimensions of the reconfigurable compact antenna. (c) Photography of the fabricated prototype. Calculated (d) and measured (e) reflection coefficients of the 8 configurations of the structure.

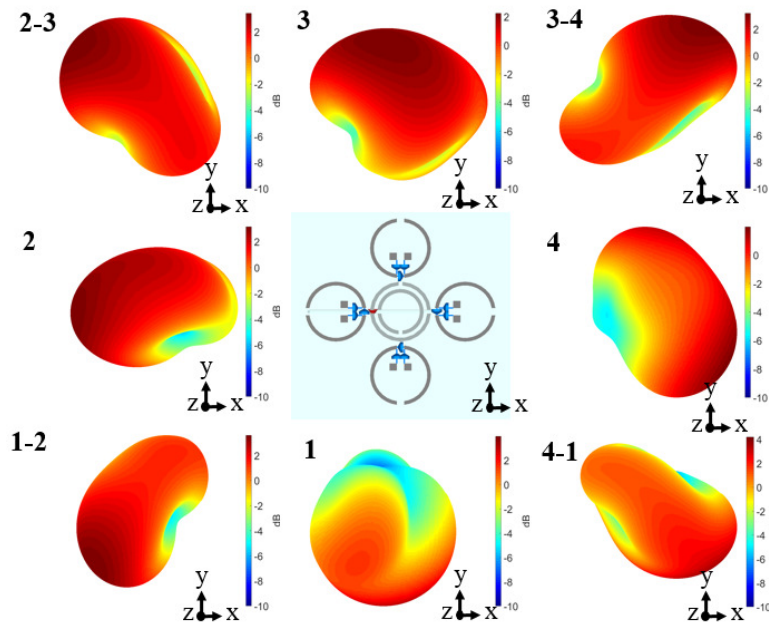


Figure 3. The three-dimensional radiation patterns (gain) of the structure calculated at 2.45 GHz.

100 MHz bandwidth (see Fig. 2(c)). As expected, the beams are oriented into 8 different directions as shown in Fig. 3.

Thanks to the low $\tan \delta$ substrate, the losses in the substrate are limited, and the radiation efficiency of the antenna is larger than -0.44 dB for all the antenna configurations. As summarized in Table 2, the antenna gain varies approximately between 2 and 4-dB because of the variation of the beamwidth. The reflection parameter (S_{11}) ranges between -22 dB and -7.7 dB. Actually our target was to achieve -10 dB for all the states which is a usual target when developing antennas. However, this target seems too restrictive for the desired 8 configurations.

Table 2. Reflection, gain and efficiency of the 8 states of the reconfigurable antenna at 2.45 GHz.

	1	1-2	2	2-3	3	3-4	4	4-1
S_{11} (dB)	-8.91	-9.05	-9.81	-15.73	-14.53	-8.74	-7.72	-21.79
G (dB)	3.44	3.62	3.16	3.43	2.24	3.19	1.98	3.76
η (dB)	-0.35	-0.44	-0.30	-0.36	-0.36	-0.40	-0.42	-0.44

4. EXPERIMENTAL REALIZATION OF THE ANTENNA

The structure is etched on a NELCO™ low loss substrate. A biasing circuit has been developed for each PIN diode as illustrated in Fig. 2(c). A resistance is used to polarize the diode while chokes are employed to prevent RF field to propagate along the DC switching lines. The designed structure is experimentally characterized in a semi-anechoic chamber. The measured reflection coefficient parameters of the 8 considered states are plotted in Fig. 2(d). A good impedance-matching of the structure for almost all these states around 2.45 GHz is achieved. A bandwidth of 100 MHz can be noticed for almost all the states. Some differences between the measured and calculated spectra are observed due to the biasing circuit and to the imperfection of the feeding circuit used in experiments which induces parasitic resonances.

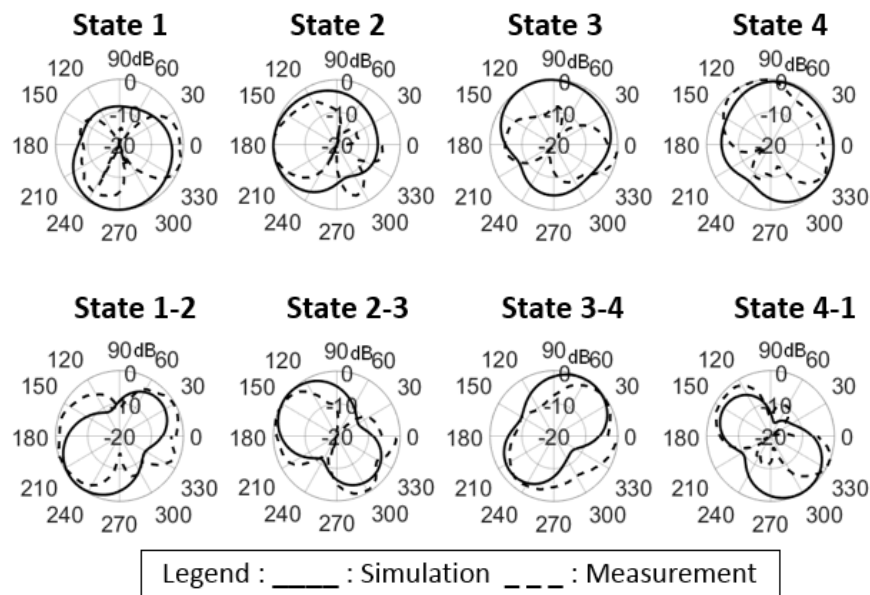


Figure 4. Simulated and measured relative polar patterns at 2.45 GHz of the 8 states of the reconfigurable SRR antenna. The numerical patterns are plotted in continuous lines while the measured ones are in dashed lines.

Due to the limitation of our anechoic chamber, only normalized radiation patterns are measured in the plane of the substrate. The 8 experimental radiation patterns are plotted in Fig. 4. They are compared to the ones obtained by simulation. Globally the main experimental lobes correspond to the simulated one. The discrepancies observed are due to the experimental conditions aforementioned.

5. SPATIAL DIVERSITY

The spatial diversity is a key point for telecommunication applications and especially for new telecommunication schemes such as Spatial Modulation communications [17]. Indeed, it quantifies the ability of the emitter to generate several uncorrelated radiation patterns that would thereafter be distinguished by an array of receivers. The lower the correlation is between the radiation patterns of the reconfigurable antenna, the better would be the performance and the robustness of the wireless communication link. To quantify this spatial diversity, we estimate the envelope correlation coefficient ECC [1].

Numerically, the ECC between the radiation patterns i and j is given by:

$$\rho_{ij}^{sim} = \frac{\left| \int \left(E_i^\theta \cdot E_j^{\theta*} + E_i^\phi \cdot E_j^{\phi*} \right) d\Omega \right|}{\sqrt{\int |E_i|^2 d\Omega \cdot \int |E_j|^2 d\Omega}} \quad (4)$$

where E_i^θ and E_i^ϕ are the inclination and azimuth far-field electric components when the reconfigurable antenna activates its state i . The calculation of these coefficients is done by integrating over a domain of 4π sr as if there is an array of receivers all around the reconfigurable antenna that probes the correlation between different patterns. Generally, the correlation factors depend strongly on the polarization, the directivity, and the phase of the complex electric fields of the radiation patterns. This parameter gives a strong indicator of the similarities between the radiated patterns. The matrix of the correlation factors is shown in Fig. 5(a). One can see that low values of correlation between the radiation patterns are obtained numerically. Here the lowest value of correlation is 3% between states 1-2 and 2-3. The highest value is 72% between states 2-3 and 4-1. The other values are mainly below 40% which is promising for implementing a reconfigurable antenna with a spatial diversity in a indoor channel.

We estimate the ECC experimentally in a reverberation chamber. A reverberation chamber advantageously replaces an anechoic chamber because the multiple reflections over the walls of a cavity

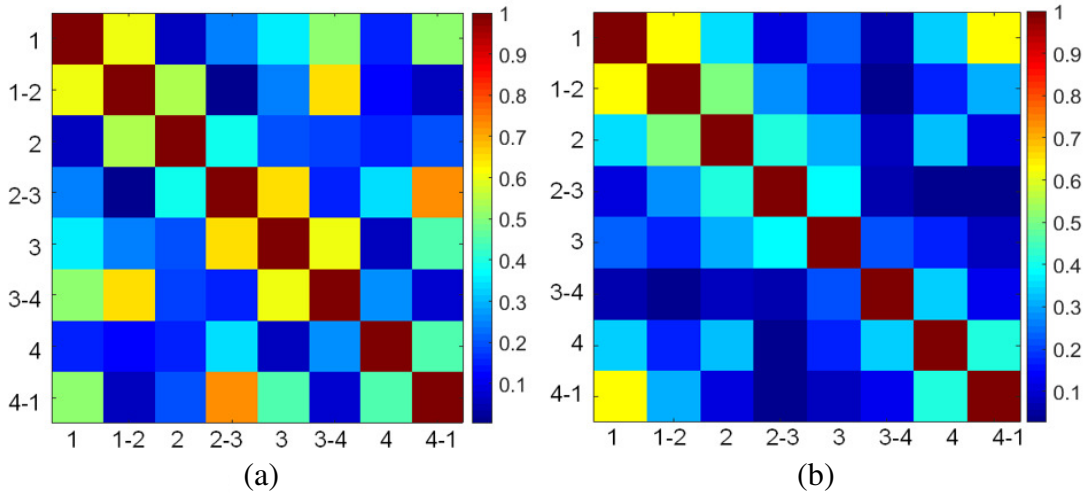


Figure 5. (a) Envelope Correlation Coefficient (ECC) simulated numerically in 3D space at 2.45 GHz. (b) Averaged correlation matrix between the different radiation patterns over all the elements of the receiver.

play the role of the multiple measurements with respect to emission direction. However, the method requires to average the field with respect to a small bandwidth (electronic mode-stirring) and with respect to the different positions of a tuner (mechanical mode-stirring). The coherence bandwidth of the used reverberating cavity is 150 kHz at the frequency of 2.4 GHz, and the stirrer has a fixed step of 36 deg. The estimation of the ECC between two states i and j is done by taking the transmission parameters S_i and S_j between the reconfigurable SRR antenna and a given element of the receiver. The expression of the correlation factor is given by:

$$C_{ij}^{rev} = \frac{\langle |S_i S_j^*| \rangle}{\langle |S_i| \rangle \langle |S_j| \rangle} \quad (5)$$

where $\langle \cdot \rangle$ represent the average over the mechanical stirrer and the frequency.

The lowest measured correlation is 2.6% between states 1-2 and 3-4. The highest value is 62% between states 1 and 4-1. These experimental values of the correlation factors obtained in the reverberation media tend to agree to the simulated one in 3D space (See Fig. 5(b)).

We have recently shown [17] that the use of spatial modulation communication with a reconfigurable antenna with less than 32% correlation between 2 radiation patterns is efficient. Many pairs of radiation patterns of our reconfigurable antenna fulfill this condition.

6. CONCLUSION

An original compact reconfigurable antenna that is able to provide a beam steering and high spatial diversity is presented in this paper. The structure has been made of a coupled system of split ring resonators. The use of the split rings has made our prototype very compact compared to the wavelength. Thanks to the use of the hybridization techniques, the proposed designed reconfigurable antenna has achieved 8 uncorrelated radiation patterns at 2.45 GHz. The averaged gain of the patterns is 3 dB. The efficiency is larger than -0.44 dB. The reflection coefficient is smaller than -7.7 dB. The spatial diversity has been validated numerically and experimentally. It can be as small as a few percent. The proposed structure should provide an interesting solution for low power communication schemes such as Spatial Modulation Communication.

ACKNOWLEDGMENT

This project has received funding from the French Project ANR Spatial Modulation (ANR-15-CE25-0016). This work is also supported by LABEX WIFI (Laboratory of Excellence within the French Program Investments for the Future) under references ANR-10-LABX-24 and ANR-10-IDEX-0001-02 PSL.

REFERENCES

1. Qin, P.-Y., Y. J. Guo, S. Member, and A. R. Weily, "A pattern reconfigurable U-slot antenna and its applications in MIMO systems," *IEEE Transactions on Antennas and Propagation*, Vol. 60, No. 1, 516–528, 2012.
2. Sarrazin, J., Y. Mahe, S. Avrillon, and S. Toutain, "Pattern reconfigurable cubic antenna," *IEEE Transactions on Antennas and Propagation*, Vol. 57, 310–317, 2009.
3. Chen, S.-H., J.-S. Row, and K.-L. Wong, "Reconfigurable square-ring patch antenna with pattern diversity," *IEEE Transactions on Antennas and Propagation*, Vol. 55, No. 2, 472–475, Feb. 2007.
4. Chen, R.-H. and J.-S. Row, "Single-fed microstrip patch antenna with switchable polarization," *IEEE Transactions on Antennas and Propagation*, Vol. 56, No. 4, 922–926, Apr. 2008.
5. Ourir, A., S. N. Burokur, R. Yahiaoui, and A. D. Lustrac, "Directive metamaterial-based subwavelength resonant cavity antennas — Applications for beam steering," *Comptes Rendus Physique*, Vol. 10, 414–422, Jun. 2009.

6. Pendry, J., A. Holden, D. Robbins, and W. Stewart, "Magnetism from conductors and enhanced nonlinear phenomena," *IEEE Transactions on Microwave Theory and Techniques*, Vol. 47, No. 11, 2075–2084, 1999.
7. Zuffanelli, S., G. Zamora, P. Aguila, F. Paredes, F. Martin, and J. Bonache, "Analysis of the split ring resonator (SRR) antenna applied to passive UHF-RFID tag design," *IEEE Transactions on Antennas and Propagation*, Vol. 64, No. 3, 856–864, Mar. 2016.
8. Alici, K. B. and E. Ozbay, "Electrically small split ring resonator antennas," *Journal of Applied Physics*, Vol. 101, 083104, Apr. 2007.
9. Cheng, X., D. E. Senior, J. J. Whalen, and Y.-K. Yoon, "Electrically small tunable split ring resonator antenna," *2010 IEEE Antennas and Propagation Society International Symposium*, 1–4, Jul. 2010.
10. Hand, T. H. and S. A. Cummer, "Controllable magnetic metamaterial using digitally addressable split-ring resonators," *IEEE Antennas and Wireless Propagation Letters*, Vol. 8, 262–265, 2009.
11. Jouvaud, C., A. Ourir, and J. de Rosny, "Adaptive metamaterial antenna using coupled tunable split-ring resonators," *Electronics Letters*, Vol. 49, 518–519, Apr. 2013.
12. Christodoulou, C. G., Y. Tawk, S. A. Lane, and S. R. Erwin, "Reconfigurable antennas for wireless and space applications," *Proceedings of the IEEE*, Vol. 100, 2250–2261, Jul. 2012.
13. Jung, C., M. Lee, G. P. Li, and F. De Flaviis, "Reconfigurable scan-beam single-arm spiral antenna integrated with rf-mems switches," *IEEE Transactions on Antennas and Propagation*, Vol. 54, No. 2, 455–463, 2006.
14. Shelley, S., J. Costantine, C. G. Christodoulou, D. E. Anagnostou, and J. C. Lyke, "Fpga-controlled switch-reconfigured antenna," *IEEE Antennas and Wireless Propagation Letters*, Vol. 9, 355–358, 2010.
15. White, C. R. and G. M. Rebeiz, "Single- and dual-polarized tunable slot-ring antennas," *IEEE Transactions on Antennas and Propagation*, Vol. 57, No. 1, 19–26, 2009.
16. Tawk, Y., A. R. Albrecht, S. Hemmady, G. Balakrishnan, and C. G. Christodoulou, "Optically pumped frequency reconfigurable antenna design," *IEEE Antennas and Wireless Propagation Letters*, Vol. 9, 280–283, 2010.
17. Phan-Huy, D.-T., Y. Kokar, K. Rachedi, P. Pajusco, A. Mokh, T. Magounaki, R. Masood, C. Buey, P. Ratajczak, N. Malhouroux-Gaffet, J.-M. Conrat, J.-C. Prevotet, A. Ourir, J. D. Rosny, M. Crussiere, M. Helard, A. Gati, T. Sarrebourg, and M. D. Renzo, "Single-carrier spatial modulation for the internet of things: Design and performance evaluation by using real compact and reconfigurable antennas," *IEEE Access*, Vol. 7, 18978–18993, 2019.